

Disk-Planet Interactions During Planet Formation

J. C. B. Papaloizou

University of Cambridge

R. P. Nelson

Queen Mary, University of London

W. Kley

Universität Tübingen

F. S. Masset

Saclay, France and UNAM Mexico

P. Artymowicz

University of Toronto at Scarborough and University of Stockholm

The discovery of close orbiting extrasolar giant planets led to extensive studies of disk planet interactions and the forms of migration that can result as a means of accounting for their location. Early work established the type I and type II migration regimes for low mass embedded planets and high mass gap forming planets respectively. While providing an attractive means of accounting for close orbiting planets initially formed at several AU , inward migration times for objects in the earth mass range were found to be disturbingly short, making the survival of giant planet cores an issue. Recent progress in this area has come from the application of modern numerical techniques which make use of up to date supercomputer resources. These have enabled higher resolution studies of the regions close to the planet and the initiation of studies of planets interacting with disks undergoing MHD turbulence. This work has led to indications of how the inward migration of low to intermediate mass planets could be slowed down or reversed. In addition, the possibility of a new very fast type III migration regime, that can be directed inwards or outwards, that is relevant to partial gap forming planets in massive disks has been investigated.

1. INTRODUCTION

The discovery of extrasolar planets around sun-like stars (51 Pegasi b) (*Mayor and Queloz, 1995; Marcy and Butler, 1995; Marcy and Butler, 1998*) has revealed a population of close orbiting giant planets with periods of typically a few days, the so called 'hot Jupiters'. The difficulties associated with forming such planets in situ, either in the critical core mass accumulation followed by gas accretion scenario, or the gravitational instability scenario for giant planet formation has led to the realisation of the potential importance of large scale migration in forming or young planetary systems.

This in turn led to more intensive theoretical development of disk protoplanet interaction theory that had already led to predictions of orbital migration (see *Lin and Papaloizou, 1993; Lin et al., 2000* and references therein). At the time of PPIV, the type I and type II migration regimes, the former applying to small mass embedded protoplanets and the latter to gap forming massive protoplanets, had become apparent. Both these regimes predicted disturbingly short radial infall times that in the type I case threatened the

survival of embryo cores in the $1 - 15M_{\oplus}$ regime before they could accrete gas to become giant planets. The main questions to be addressed were how to resolve the type I migration issue and to confirm that type II migration applicable to giant planets could indeed account for the observed radial distribution and the hot Jupiters.

Here, we review recent progress in the field of disk planet interactions in the context of orbital migration. For reasons of space constraint we shall not consider the problem of excitation or damping of orbital eccentricity. The most recent progress in this area has come from carrying out large scale two and three dimension simulations that require the most up to date supercomputer resources. This has enabled the study of disk planet interactions in disks undergoing MHD turbulence, the study of the regions close to the planet using high resolution multigrid techniques, led to suggestions for the possible resolution of the type I issue and revealed another possible type III migration regime. However, the complex nature of these problems makes them challenging numerically and as a consequence numerical convergence has not been attained in some cases.

In sections 2, 3, and 4 we review type I migration, type II

migration and type III migration respectively. In section 5 we review recent work on disk planet interactions in disks with MHD turbulence and in section 6 we give a summary.

2. TYPE I MIGRATION

When the mass of the protoplanet is small the response it induces in the disk can be calculated using linear theory. When the disk flow is non magnetic and laminar, density waves propagate both outwards and inwards away from the protoplanet. These waves carry positive and negative angular momentum respectively and accordingly a compensating tidal torque is applied to the orbit resulting in type I migration.

2.1. The tidal torque

The problem of determining the evolution of the planet orbit amounts to an evaluation of tidal torques. For a sufficiently small planet mass (an upper limit of which will be specified below) one supposes that the gravitational potential of the protoplanet forces small perturbations. The hydrodynamic equations are then linearized about a basic state consisting of an unperturbed axisymmetric accretion disk and the response calculated. The gravitational potential ψ of a proplanet in circular orbit is expressed as a Fourier series in the form

$$\psi(r, \varphi, t) = \sum_{m=0}^{\infty} \psi_m(r) \cos\{m[\varphi - \omega_p t]\}, \quad (1)$$

where φ is the azimuthal angle and $2\pi/(\omega_p)$ is the orbital period of the planet of mass M_p at orbital semi-major axis a . The total torque acting on the disk is given by $\Gamma = -\int_{Disk} \Sigma \vec{r} \times \nabla \psi d^2r$ where Σ is the surface density of the disk.

An external forcing potential $\psi_m(r, \varphi)$ with azimuthal mode number m that rotates with a pattern frequency ω_p in a disk with angular velocity $\Omega(r)$ triggers a response that exchanges angular momentum with the orbit whenever, neglecting effects due to pressure, $m(\Omega - \omega_p)$ is equal either 0 or $\pm\kappa$, with, for a Keplerian disk to adequate accuracy, $\kappa \equiv \Omega$ being the epicyclic frequency. The first possibility occurs when $\Omega = \omega_p$ and thus corresponds to a corotation resonance. The second possibility corresponds to an inner Lindblad resonance located inside the orbit for $\Omega = \omega_p + \kappa/m$ and an outer Lindblad resonance outside the orbit for $\Omega = \omega_p - \kappa/m$.

2.1.1. Torques at Lindblad resonances. Density waves are launched at Lindblad resonances and as a consequence of this a torque acts on the planet. It is possible to solve the wave excitation problem using the WKB method. In that approximation an analytic expression for the torque can be found. The torque arising from the component of the potential with azimuthal mode number m is found, for a Keplerian disk, to be given by

$$\Gamma_m^{LR} = \frac{\text{sign}(\omega_p - \Omega)\pi^2\Sigma}{3\Omega\omega_p} \Psi^2, \quad (2)$$

with

$$\Psi = r \frac{d\psi_m}{dr} + \frac{2m^2(\Omega - \omega_p)}{\Omega} \psi_m. \quad (3)$$

where the expression has to be evaluated at the location of the resonance.

The derivation of this torque formula in the context of satellite(planet)- interaction with a gaseous disk can be found in (Goldreich and Tremaine, 1979; Lin and Papaloizou, 1979; Lin and Papaloizou, 1993). In a Keplerian disk, the torque exerted on the planet from an outer Lindblad resonance is negative corresponding to a drag, and the torque due to an inner Lindblad resonance is positive corresponding to an acceleration.

The total torque may be obtained by summing contributions over m . However, when doing so it must be borne in mind that the above analysis, appropriate to a cold disk, is only valid when $\xi = mc_s/(r\Omega) \ll 1$,

For finite ξ the positions of the Lindblad resonances are modified, being now given by

$$m^2(\Omega - \omega_p)^2 = \Omega^2(1 + \xi^2), \quad (4)$$

where c_s is the sound speed.

The effective positions of the resonances are shifted with respect to the cold disk case. In particular, noting that $c_s = H\Omega$, with $H \ll r$, being the disk semithickness one sees that when $m \rightarrow \infty$, Lindblad resonances pile up at

$$r = a \pm \frac{2H}{3}. \quad (5)$$

Physically these locations correspond to where the disk flow relative to the planet becomes sonic so that they are naturally the points from where the density waves are first launched (Goodman and Rafikov, 2001).

In addition a correction factor has to be applied to the expression for the torque acting on the disk which now reads (see Artymowicz, 1993; Ward, 1997; Papaloizou and Larwood, 2000)

$$\Gamma_m^{LR} = \frac{\text{sign}(\omega_p - \Omega)\pi^2\Sigma}{3\Omega\omega_p\sqrt{1 + \xi^2(1 + 4\xi^2)}} \Psi^2. \quad (6)$$

This together with the shift in Lindblad resonance locations ensures that when contributions are summed over m , they decrease rapidly for $\xi \gg 1$, a phenomenon known as the torque cut off.

2.1.2. Differential Lindblad torque. The total outer (resp. inner) Lindblad torque are obtained by summing over all individual components.

$$\Gamma_{OLR(ILR)} = \sum_{m=1(2)}^{+\infty} \Gamma_m^{OLR(ILR)}, \quad (7)$$

These are referred to as one-sided Lindblad torques. They scale with h^{-3} , where $h = H/r$ is the disk aspect ratio (Ward, 1997).

In Fig. 1 one can see that the torque cut-off occurs at larger m values in the thinner disk (the outer torque value

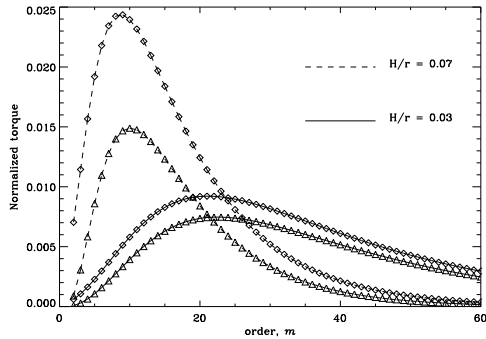


Fig. 1.— Individual inner and outer torques (in absolute value) in a $h = 0.07$ and $h = 0.03$ disk, as a function of m . For each disk thickness, the upper curve (diamonds) shows the outer torque and the lower one (triangles) the inner torque. These torques are normalized to $\Gamma_0 = \pi q^2 \Sigma a^4 \omega_p^2 h^{-3}$.

peaks around $m \sim 8-9$ for $h = 0.07$, while it peaks around $m \sim 21-22$ for $h = 0.03$). Also, there is for both disk aspect ratios a very apparent mismatch between the inner and the outer torques, the former being systematically smaller than the later. If we consider the torque of the disk acting on the planet, then the outer torques are negative and the inner ones positive, and the total torque is therefore negative. As a consequence *migration is directed inwards* and leads to a decay of the orbit onto the central object (Ward, 1997). It can be shown that the relative mismatch of inner and outer torques scales with the disk thickness (Ward, 1997). Since one-sided torques scale as h^{-3} , the migration rate scales with h^{-2} .

There are several reasons for the torque asymmetry which conspire to make the differential Lindblad torque a sizable fraction of the one-sided torque in a $h = O(10^{-1})$ disk (Ward, 1997). Most importantly, for a given m value, the inner Lindblad resonances lie further from the orbit than the corresponding outer Lindblad resonances. From this it follows that the relative disk motion becomes sonic further away inside the orbit making the launching of density waves less efficient in the inner regions. Note that the net torque on the disk is positive making that on the planet negative so producing inward migration. This is found to be the case for disks with reasonable density profiles (see Eq. (9) below).

2.1.3. Linear corotation torque. The angular momentum exchange at a corotation resonance corresponds to different physical processes than at a Lindblad resonance. At the latter the perturbing potential tends to excite epicyclic motion, and, in a protoplanetary disk, the angular momentum deposited is evacuated through pressure supported waves. On the contrary, these waves are evanescent in the corotation region, and are unable to remove the angular momentum brought by the perturber (Goldreich and Tremaine, 1979).

The corotation torque exerted on a disk by an external

perturbing potential with m fold symmetry is given by

$$\Gamma_m^{\text{CR}} = \frac{m\pi^2\psi^2}{2(d\Omega/dr)} \frac{d}{dr} \left(\frac{\Sigma}{B} \right), \quad (8)$$

to be evaluated at the corotation radius. ψ is the amplitude of the forcing potential, and $B = \kappa^2/(4\Omega)$ the second Oort's constant. Since B is half the flow vorticity, the corotation torque scales with the gradient of (the inverse of) the specific vorticity, sometimes also called the vortensity. The corotation torque therefore cancels out in a $\Sigma \propto r^{-3/2}$ disk, such as the standard minimum mass solar nebula with $h = 0.05$ (MMSN).

In most cases, a disk sharp edge being a possible exception, the corotation torque can be safely neglected when estimating the migration timescale in the linear regime. Indeed, even the fully unsaturated corotation torque amounts at most to a few tens of percent of the differential Lindblad torque (Ward, 1997; Tanaka et al., 2002), while Korycansky and Pollack (1993) find through numerical integrations that the corotation torque is an even smaller fraction of the differential Lindblad torque than given by analytical estimates.

2.1.4. Nonlinear effects. In a frame which corotates with the perturbation pattern, if inviscid, the flow in the neighborhood of corotation consists of libration islands, in which fluid elements librate on closed streamlines, between regions in which fluid elements circulate in opposite senses. This is true for general perturbations and not just those with m fold symmetry. See, e.g., fig. 2 which applies to the corotation or coorbital region associated with a planet in circular orbit. In linear theory, the period of libration, which tends to infinity as the perturbation amplitude (or planet mass) tends to zero, is such that complete libration cycles do not occur and angular momentum exchange rates are appropriate only to sections at definite radial locations.

However, in actual fact, fluid elements in the libration region exchange zero net angular momentum with the perturbation during one complete libration cycle. Accordingly if a steady state of this type can be set up, in full non linear theory the net corotation torque is zero. When this is the case the corotation resonance is said to be saturated.

But note that, when present, viscosity can cause an exchange of angular momentum between librating and circulating fluid elements which results in a net corotation torque. Then saturation is prevented. This is possible if the viscous timescale across the libration islands is smaller than the libration time (see Goldreich and Sari, 2003; Ogilvie and Lubow, 2003). It is found that for small viscosity, the corotation torque is proportional to ν (Balmforth and Korycansky, 2001), while at large viscosity one obtains the torque induced as material flowing through the orbit passes by the perturbing planet (Masset, 2001).

Note that these saturation properties are not captured by a linear analysis, since saturation requires a finite libration time, hence a finite resonance width. In the linear limit, the corotation torque appears as a discontinuity at corotation of the advected angular momentum flux, which corresponds to infinitely narrow, fully unsaturated libration islands.

2.2. Type I migration drift rate estimates

There are a number of estimates of the Type I migration rate in the literature that are based on summing resonant torque contributions (see *Ward, 1997; Papaloizou and Larwood, 2000* and references therein). Calculations using 2D models have to soften the planet potential to obtain agreement with results obtained from 3D calculations but such agreement may be obtained for reasonable choices of the softening parameter (see *Papaloizou and Terquem, 2006*).

The most recent linear calculations by *Tanaka et al. (2002)* that take into account 3D effects, and are based upon the value of the total tidal torque, including the corotation torque (fully unsaturated since it is a linear estimate), give

$$\tau \equiv a/\dot{a} = (2.7 + 1.1\alpha)^{-1} \frac{M_*^2}{M_p \Sigma a^2} h^2 \omega_p^{-1}, \quad (9)$$

for a surface density profile $\Sigma \propto r^{-\alpha}$. For an Earth-mass planet around a solar mass star at $r = 1$ AU, in a disk with $\Sigma = 1700 \text{ g cm}^{-2}$ and $h = 0.05$, this translates into $\tau = 1.6 \cdot 10^5$ years.

This semi-analytic estimate has been verified by means of 3D numerical simulations (*Bate et al., 2003; D'Angelo et al., 2003a*). Both find an excellent agreement in the limit of low-mass, thus they essentially validate the linear analytical estimate. However, while *Bate et al. (2003)* find agreement with the linear results for all planet masses, *D'Angelo et al. (2003a)* find very long migration rates for intermediate masses, i.e. for Neptune-sized objects (see Fig. 3). Additional 2d and 3D high resolution numerical simulations by *Masset et al. (2006)* show that this *migration offset* from the linear results is a robust phenomenon whose strength varies *i)* with departure from the $\Sigma \propto r^{-3/2}$ relation, *ii)* with the value of the viscosity, and *iii)* with the disk thickness. The transition from linear to the offset regime is apparently caused by the onset of non-linear effects that could be related to corotation torques whose strength also increase with departure from $\Sigma \propto r^{-3/2}$ (see section 2.1.3).

The type I migration time scale is very short, much

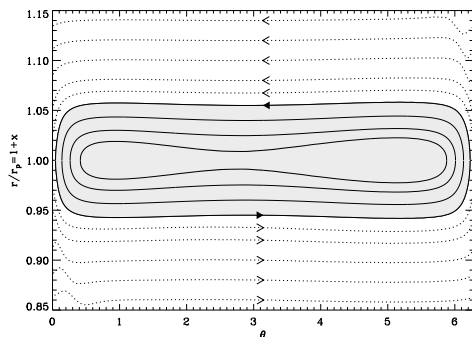


Fig. 2.— Horseshoe region with closed streamlines as viewed in a frame corotating with a planet in circular orbit (shaded area). The planet is located at $r = 1$ and $\theta = 0$ or 2π .

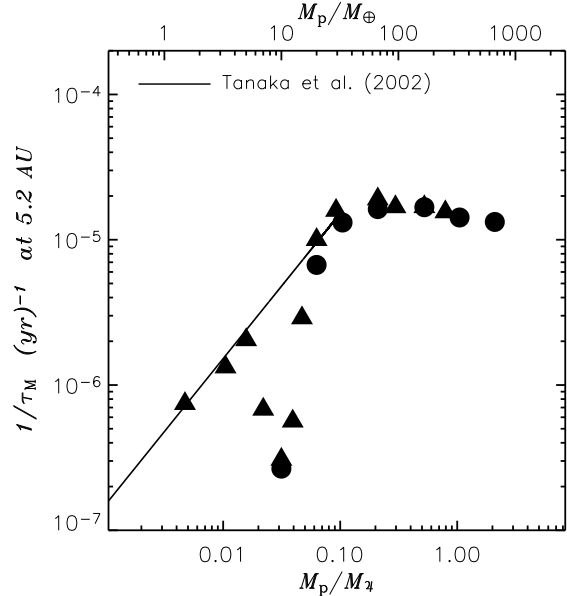


Fig. 3.— The migration rate for different planet masses for 3D fully non-linear nested grid simulations. The symbols denote different approximations (smoothing) for the potential of the planet. The solid line refers to linear results for Type I migration by *Tanaka et al., (2002)*, see Eq. 9. Figure adapted from *D'Angelo et al. (2003)*.

shorter than the build up time of the $M_p \sim 5 - 15 M_{\oplus}$ solid core of a giant planet (see, e.g., *Papaloizou and Nelson, 2005* for a discussion). Hence, the existence of type I migration makes potential difficulties for the accumulation scenario for these massive cores. This remains a problem within the framework of planet formation theory (see the discussion below for possible resolutions).

The influence of the disk's self-gravity on type I migration has been analyzed through numerical and semi-analytical methods (*Nelson and Benz, 2003; Pierens and Huré, 2003*). It increases the migration rate but the effect is small for typical disk parameters.

Papaloizou and Larwood (2000) incorporate a non zero planet eccentricity in their torque calculations and find that in general the torques weaken with increasing eccentricity and can even reverse once the eccentricity exceeds h by some factor of order unity. Thus a process that maintains eccentricity could potentially help to stall the migration process. A similar effect occurs if the disk has a global non axisymmetric distortion such as occurs if it has a finite eccentricity. This can also result in a weakening of the tidal interaction and a stalling of the torques under appropriate conditions (see *Papaloizou, 2002*).

Recent attempts to include more detailed physics of the protoplanetary disk, such as opacity transitions and their impact on the disk profile (*Menou and Goodman, 2004*), or radiative transfer and the importance of shadowing in the planet vicinity (*Jang-Condell and Sasselov, 2005*), have lead to lower estimates of the type I migration rates which

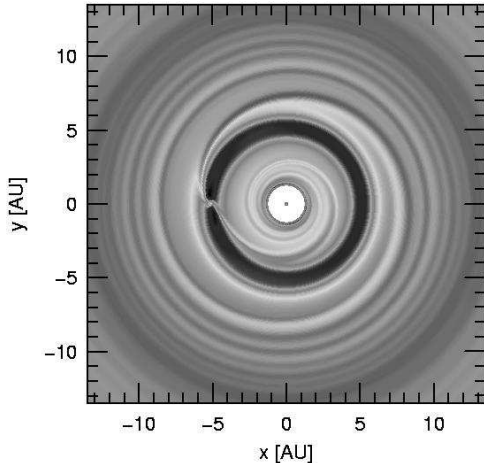


Fig. 4.— Surface density profile for an initially axisymmetric disk model two hundred orbital orbits after the introduction of a planet that subsequently remains on a fixed circular. The mass ratio is 10^{-3} .

might help resolve the accretion/migration timescale discrepancy. The aforementioned offset and also effects due to magnetic fields (see, e.g., *Terquem*, 2003) and their associated turbulence (see below) may help to extend the type I migration time scale and allow proto giant planet cores to form.

3. TYPE II MIGRATION

When the planet grows in mass the disk response cannot be treated any longer as a linear perturbation. The flow perturbation becomes non-linear and the planetary wake turns into a shock in its vicinity. Dissipation by these shocks as well as the action of viscosity leads to the deposition of angular momentum, pushes material away from the planet and a gap opens. The equilibrium width of the gap is determined by the balance of gap-closing viscous and pressure forces and gap-opening gravitational torques.

To obtain rough estimates, the condition that the planet's gravity be strong enough to overwhelm pressure in its neighbourhood is that the radius of the Hill sphere exceed the disk semi-thickness or

$$a \left(\frac{M_p}{3M_*} \right)^{1/3} > H. \quad (10)$$

The condition that angular momentum transport by viscous stresses be interrupted by the planetary tide is approximately

$$\left(\frac{M_p}{M_*} \right) > (40a^2\Omega)/\nu. \quad (11)$$

For more discussion of these aspects of gap opening, see the review by *Lin and Papaloizou* (1993), *Bryden et al.* (1999), and also *Crida et al.* (2006).

Interestingly for the standard parameters, $h = 0.05$, and $\nu/(a^2\Omega) = 10^{-5}$, (10) gives $M_p/M_* > 3.75 \times 10^{-4}$, while

(11) gives $M_p/M_* > 4 \times 10^{-4}$. Note that this result obtained from simple estimates is in good agreement with that obtained from Fig. 3.

Accordingly, for typical protoplanetary disk parameters, we can expect that a planet with a mass exceeding that of Saturn will begin to open a visible gap. Using Eq. (9) for the type I migration rate together with Eq. (10), we can estimate the minimum drift time at the marginal gap opening mass to be given by

$$(a/\dot{a}) = 3^{-2/3}(5.4 + 2.2\alpha)^{-1} \left(\frac{M_p}{M_*} \right)^{-1/3} \frac{M_*}{\pi\Sigma a^2} P_{orb}, \quad (12)$$

with P_{orb} being the orbital period. For a minimum mass solar nebula with $4\pi\Sigma a^2 = 2 \times 10^{-3}M_*$, and $M_p/M_* = 4 \times 10^{-4}$ at $5.2 au$, this gives a minimum drift time of only $\sim 3 \times 10^4 y$. This simply obtained estimate is in good agreement with the results presented in Fig. 3.

3.1. Numerical modelling

Currently, heavy reliance is placed on numerical methods to analyse the dynamics of the planet-disk interaction, the density structure of the disk, and the resulting gravitational torques acting on the planet. The corresponding migration regime is called Type II migration (e.g., *Lin and Papaloizou*, 1986; *Ward*, 1997).

The first modern hydrodynamical calculations of planet-disk interaction in the Type II regime were performed by *Bryden et al.* (1999), *Kley* (1999), *Lubow et al.* (1999). Since protoplanetary accretion disks are assumed to be vertically thin, these first simulations used a two-dimensional ($r - \varphi$) model of the accretion disk. The vertical thickness H of the disk is incorporated by assuming a given radial temperature profile $T(r) \propto r^{-1}$ which makes the ratio H/r constant. Typically the simulations assume $H/r = 0.05$ so that at each radius, r , the Keplerian speed is 20 times faster than the local sound speed. Initial density profiles typically have power laws for the surface density $\Sigma \propto r^{-s}$ with s between 0.5 and 1.5. More recently, fully 3D models have been calculated. These have used the same kind of isothermal equation of state (*Bate et al.*, 2003; *D'Angelo et al.*, 2003a).

The viscosity is dealt with by solving the Navier Stokes equations with the kinematic viscosity ν taken as constant or given by an α -prescription $\nu = \alpha c_s H$, where α is a constant. From observations of protostellar disks, values lying between 10^{-4} and 10^{-2} are inferred for the α -parameter but there is great uncertainty. Full MHD-calculations have shown that the viscous stress-tensor ansatz may give (for sufficiently long time averages) a reasonable approximation to the *mean* flow in a turbulent disk (*Papaloizou and Nelson*, 2003). The embedded planets are assumed to be point masses (using a smoothed or softened potential). The disk influences their orbits through gravitational torques which cause orbital evolution. The planets may also accrete mass from the surrounding disk (*Kley*, 1999).

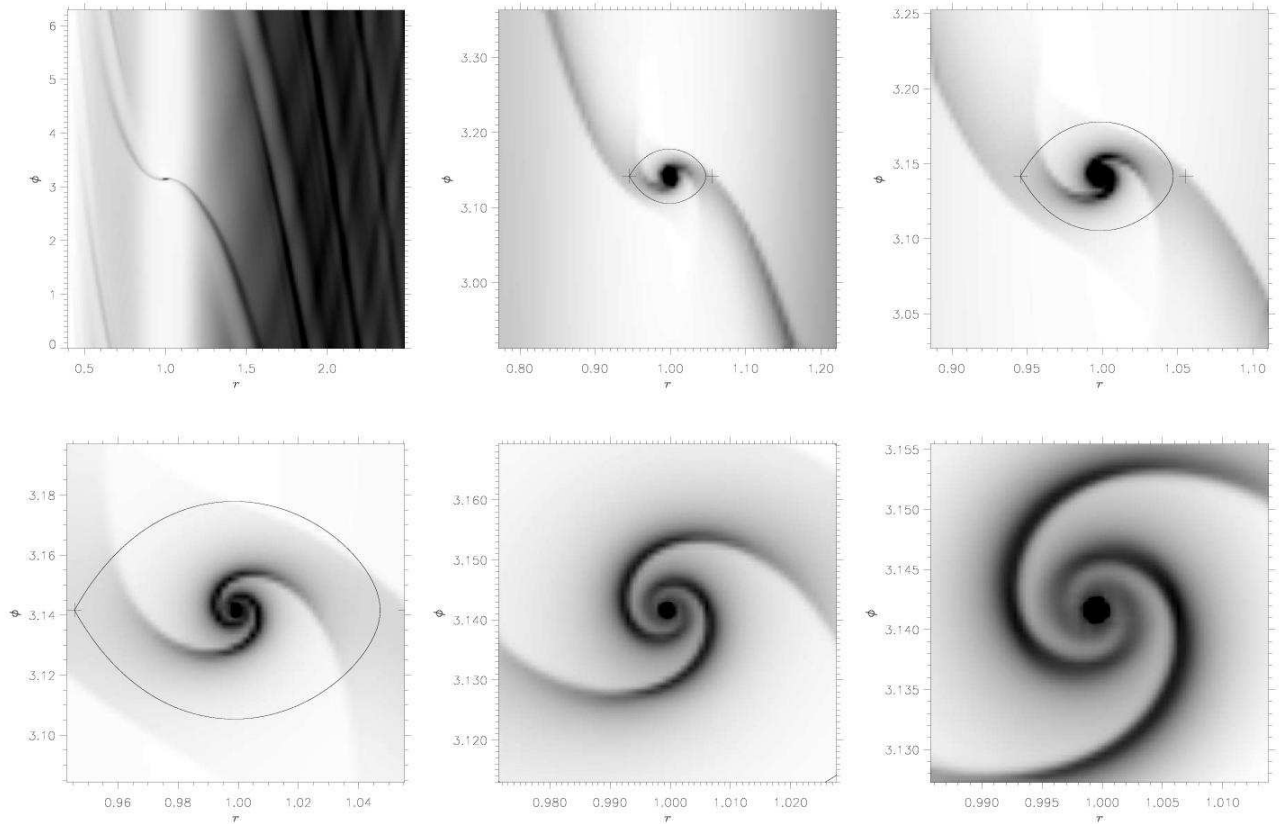


Fig. 5.— Density Structure of a $1M_{Jup}$ on each level of the nested grid system, consisting of 6 grid levels in total. The top left panel displays the total computational domain. The line indicates the size of the Roche lobe.

3.2. Viscous laminar Disks

The type of modeling outlined in the previous section yields in general smooth density and velocity profiles, and we refer to those models as *viscous laminar disk* models, in contrast to models which do not assume an a priori given viscosity and rather model the turbulent flow directly (see below).

A typical result of such a viscous computation obtained with a 128×280 grid (in $r - \varphi$) is displayed in Fig. 4. Here, the planet with mass $M_p = 1M_{Jup}$ and semi-major axis $a_p = 5.2AU$ is *not* allowed to move and remains on a fixed circular orbit, an approximation which is made in many simulations. Clearly seen are the major effects an embedded planet has on the structure of the protoplanetary accretion disk. The gravitational force of the planet leads to spiral wave patterns in the disk. In the present calculation (Fig. 4) there are two spirals in the outer disk and in the inner disk. The tightness of the spiral arms depends on the temperature (i.e. h) of the disk. The smaller the temperature the tighter the spirals. The density gap at the location of the planet discussed above is also visible.

To obtain more insight into the flow near the planet and to calculate accurately the torques of the disk acting on the planet, the nested-grid approach described above has been

used together with a variable grid-size. (*D'Angelo et al., 2002; Bate et al., 2003; D'Angelo et al., 2003a*). Such a grid-system is fixed and therefore not adaptive. The planet is located at the center of the finest grid.

The result for a 2D computation using 6 grids is displayed in Fig. 5, for more details see also *D'Angelo et al. (2002)*. The top left base grid has a resolution of 128×440 and each sub-grid has a size of 64×64 with a refinement factor of two from level to level. It is noticeable that the spiral arms inside the Roche-lobe of a high mass planet are detached from the global outer spirals. The top right hand panel of figure 5 indicates that the outer spirals fade away exterior to the one around the planet. The two-armed spiral around the planet extends deep inside the Roche-lobe and enables the accretion of material onto the planet. The nested-grid calculations have recently been extended to three dimensions (3D) and a whole range of planetary masses has been investigated (*D'Angelo et al., 2003a*). In the 3D case the spiral arms are weaker and accretion occurs primarily from regions above and below the midplane of the disk.

3.3. The migration rate

Such high-resolution numerical computations allow for a detailed computation of the torque exerted by the disk ma-

terial onto the planet, and its mass accretion rate. For migration rates see Fig. 3.

The consequences of accretion and migration have been studied by numerical computations which do not hold the planet fixed at some radius but rather follow the orbital evolution of the planet (Nelson *et al.*, 2000), allowing planetary growth. The typical migration and accretion timescales are of the order of 10^5 yrs, while the accretion timescale may be slightly smaller. This is in very good agreement with the estimates obtained from the models using a fixed planet. These simulations show that during their inward migration they grow up to about $4 M_{Jup}$.

The inward migration time of 10^5 yrs can be understood as the natural viscous evolution time of the local accretion disk. When the planet mass is not too large, and it makes a gap in the disk, it tends to move as a disk gas particle would and thus move inwards on the viscous timescale $\tau \sim a^2/\nu$, (Lin and Papaloizou, 1986). But note that when the mass of the planet exceeds the disk mass in its neighbourhood on a scale a , the migration rate decreases because of the relatively large inertia of the planet (see, e.g., Syer and Clarke, 1995; Ivanov, Papaloizou and Polnarev, 1999).

The consequence of the inclusion of thermodynamic effects (viscous heating and radiative cooling) on the gap formation process and type II migration has been studied by D'Angelo *et al.*, (2003b). In two-dimensional calculations an increased temperature in the circumplanetary disk has been found. This has interesting consequences for the possible detection of an embedded protoplanet. The effect that self-gravity of the disk has on migration has been analysed through numerical simulations (Nelson and Benz, 2003). For typically expected protostellar disk masses the influence is rather small.

3.4. Consequences for evolution in young planetary systems

A number of studies with the object of explaining the existence and distribution of giant planets interior to the 'snow line' at $2au$ which make use of type II migration have been performed (e.g., Trilling *et al.*, 1998; 2002; Armitage *et al.* 2002; Alibert *et al.* 2004; Ida and Lin, 2004). These assume formation beyond the snow line followed by inward type II migration that is stopped by one of: disk dispersal, Roche lobe overflow, stellar tides or entering a stellar magnetospheric cavity. Reasonable agreement with observations is attained. But type I migration has to be suppressed possibly by one of the mechanisms discussed in this review.

4. TYPE III MIGRATION

The terminology type III migration refers to migration for which an important driver is material flowing through the coorbital region. Consider an inwardly (resp. outwardly) migrating planet. Material of the inner disk (resp. outer disk) has to flow across the co-orbital region and it executes one U-turn in the horseshoe region (see Fig. 2) to do so. By doing this, it exerts a corotation torque on the planet

that scales with the migration rate. (see Masset and Papaloizou, 2003; Artymowicz, 2004; Papaloizou, 2005) for further analysis and discussion).

The specific angular momentum that a fluid element near the separatrix takes from the planet when it switches from an orbit with radius $a - x_s$ to $a + x_s$ is $\Omega a x_s$ where x_s is the radial half width of the horseshoe region estimated to be 2.5 Hill sphere radii (Artymowicz, 2006).

The torque exerted on a planet migrating at a rate \dot{a} by the inner or outer disk elements as they cross the planet orbit on a horseshoe U-turn is accordingly, to lowest order in x_s/a :

$$\Gamma_2 = (2\pi a \Sigma_s \dot{a}) \cdot (\Omega a x_s), \quad (13)$$

where Σ_s is the surface density at the upstream separatrix. The system of interest for the evaluation of the sum of external torques is composed of the planet, all fluid elements trapped in libration in the horseshoe region (with mass M_{HS}) and the Roche lobe content (with mass M_R), because these components migrate together.

The drift rate of this system is then given by

$$\frac{1}{2}(M_p + M_{HS} + M_R) \cdot (\Omega \dot{a}) = (4\pi a x_s \Sigma_s) \cdot \frac{1}{2}(\Omega a \dot{a}) + \Gamma_{LR} \quad (14)$$

which can be rewritten as

$$M'_p \cdot \frac{1}{2}(\Omega \dot{a}) = (4\pi a \Sigma_s x_s - M_{HS}) \cdot \frac{1}{2}(\Omega a \dot{a}) + \Gamma_{LR}, \quad (15)$$

where $M'_p = M_p + M_R$ is all of the mass content within the Roche lobe, which from now on for convenience we refer to as the planet mass. The first term in the first bracket of the r.h.s. of Eq (15) corresponds to the horseshoe region surface multiplied by the upstream separatrix surface density, hence it is the mass that the horseshoe region would have if it had a uniform surface density equal to the upstream surface density. The second term is the actual horseshoe region mass. The difference between these two terms is called in Masset and Papaloizou (2003) the coorbital mass deficit and denoted δm . Thus we have

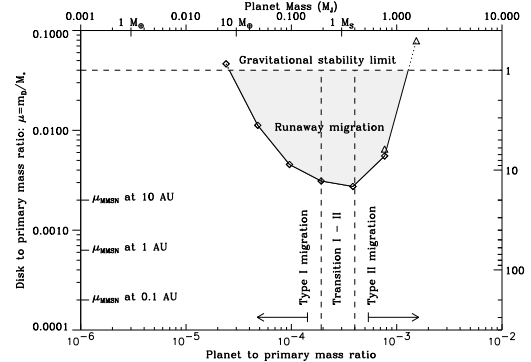


Fig. 6.— Runaway limit domain for a $H/R = 0.04$ and $\nu = 10^{-5}$ disk, with a surface density profile $\Sigma \propto r^{-3/2}$. The variable $m_D = \pi \Sigma r^2$ features on the y axis. It is meant to represent the local disk mass, and it therefore depends on the radius.

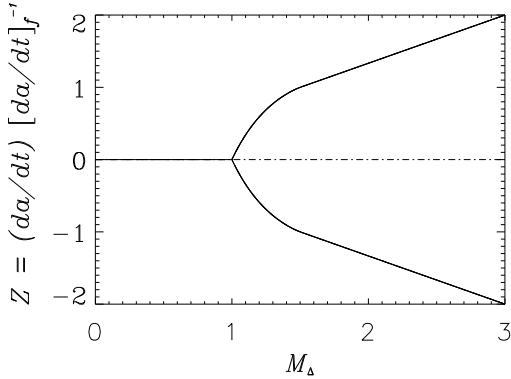


Fig. 7.— Bifurcation diagram derived from equation (21). This is extended to negative $\frac{da}{dt}$ by making the curve symmetric about the M_Δ axis. The bifurcation to fast migration occurs for $M_\Delta = 1$.

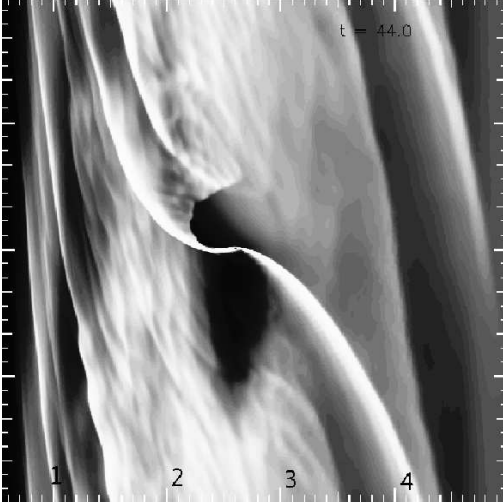


Fig. 8.— This is a density contour plot taken from a PPM simulation with variable adaptive mesh of a Jupiter mass planet in a disk 2.5 times more massive than the minimum mass solar nebula (see Artymowicz, 2006). The planet after being placed on a positive density gradient, increased its semi-major axis by a factor of 2.6 in only 44 orbits. A trapped coorbital low density region is clearly visible and the migration speed corresponds to $M_\Delta \approx 3$.

$$\frac{1}{2}\dot{a}\Omega a(M'_p - \delta m) = \Gamma_{LR} \quad (16)$$

Eq (16) gives a drift rate

$$\dot{a} = \frac{2\Gamma_{LR}}{\Omega a(M'_p - \delta m)} \quad (17)$$

This drift rate is faster than the standard estimate in which one neglects δm . This comes from the fact that the coorbital dynamics alleviates the differential Lindblad torque task by advecting fluid elements from the upstream to the downstream separatrix. The angular momentum exchanged with the planet by doing so produces a positive feedback on its migration.

As δm tends to M'_p , most of the angular momentum change of the planet and its coorbital region is balanced by that of the orbit crossing circulating material, making migration increasingly cost effective.

When $\delta m \geq M'_p$, the above analysis, assuming a steady migration (\dot{a} constant), is no longer valid. Migration may undergo a runaway leading to a strongly time varying migration rate. Runaway (also denoted type III or fast) migration is therefore a mode of migration of planets that deplete their coorbital region and are embedded in sufficiently massive disks, so that the above criterion be satisfied. The critical disk mass above which a planet of given mass undergoes a runaway depends on the disk parameters (aspect ratio and effective viscosity). The limit has been considered by *Masset and Papaloizou* (2003) for different disk aspect ratios and a kinematic viscosity $\nu = 10^{-5}$. The type III migration domain that was found for a disk with $H/r = 0.04$ is indicated in figure 6.

Once the migration rate becomes fast enough that the planet migrates through the coorbital region in less than a libration period, the analysis leading to equation (16) becomes invalid. A recent analysis by *Artymowicz* (2006) indicates how this equation should be modified when this occurs. Consider the torque term

$$\dot{a}\Omega a\delta m/2$$

in equation (16) above. This can be regarded as the corotation torque. It can be thought of as generated as follows. Material enters the horseshoe region close to and behind the planet from the region into which the planet migrates at a maximum radial separation corresponding to the full half width x_s . However, the turn at the opposite side of the horseshoe region 2π round in azimuth occurs at a reduced maximum radial separation $x_s - \Delta$ due to the radial migration of the planet. Consideration of Keplerian circular orbits gives (*Artymowicz, 2006*)

$$\Delta = x_s \left(1 - \sqrt{1 - |\dot{a}|\dot{a}_f^{-1}} \right), \quad (18)$$

where

$$\frac{\dot{a}_f}{a} = \frac{3x_s^2}{8\pi a^2}\Omega \quad (19)$$

gives the critical or fast migration rate for which the horseshoe region can just extend the full 2π in azimuth. For larger drift rates it contracts into a tadpole like region and the dynamics is no longer described by the above analysis. Instead we should replace the square root in (18) by zero. For smaller drift rates, the torques exerted at the horseshoe turns on opposite sides of the planet are proportional to x_s^3 and $(x_s - \Delta)^3$ respectively. This is because these torques are proportional to the product of the flow rate, specific angular momentum transferred and the radial width, each of them also being proportional to the radial width. As these torques act in opposite senses, the corotation torque should be proportional to $x_s^3 - (x_s - \Delta)^3$, or $x_s^3(1 - (1 - |\dot{a}|\dot{a}_f^{-1})^{3/2})$. Note that this factor, which applies to both librating and non librating material, being $(3/2)x_s^3|\dot{a}|\dot{a}_f^{-1}$ for small drift rates, provides a match to equation (16) provided the \dot{a} multiplying δm is replaced by $(2/3)\dot{a}_f \text{sign}(\dot{a})(1 - (1 - |\dot{a}|\dot{a}_f^{-1})^{3/2})$.

Equation (16) then becomes

$$\frac{1}{2}\Omega a(M_p'\dot{a} - \frac{2}{3}\delta m\dot{a}_f \text{sign}(\dot{a})(1 - (1 - |\dot{a}|\dot{a}_f^{-1})^{3/2})) = \Gamma_{LR}. \quad (20)$$

Interestingly, when Lindblad torques are small, equation (20) now allows for the existence of steady fast migration rates which can be found by setting the left hand side to zero. Assuming without loss of generality that $\dot{a} > 0$, and setting $Z = \dot{a}/\dot{a}_f$, these states satisfy

$$Z = (2/3)M_\Delta(1 - (1 - Z)^{3/2}), \quad (21)$$

with $M_\Delta = (\delta m/M_p')$. Equation (21) gives rise to a bifurcation from the solution $Z = 0$ to fast migration solutions when $M_\Delta > 1$ or when the coorbital mass deficit exceeds the planet mass (see Figure 7). The 'fast' rate, $Z = 1$, occurs when $M_\Delta = 3/2$. For larger M_Δ , $Z = 2M_\Delta/3$.

Fast migration, for the same disk profile and planet mass, can be directed either outwards or inwards, depending on the initial conditions. This type of planetary migration is found to depend on its migration history, the "memory" of this history being stored in the way the horseshoe region is populated, i.e. in the preparation of the coorbital mass deficit. Note that owing to the strong variation of the drift rate, the horseshoe streamlines are not exactly closed, so that the coorbital mass deficit can be lost and the runaway can stall. This has been observed in some numerical simulations, whereas others show sustained fast migration episodes for Saturn or Jovian mass planets that can vary the semi-major axis by large factors in less than 100 orbits (e.g., see Figure 8). To date, it is still unclear how long such episodes can last for, and what are the conditions, if any, for them to stall or to be sustained for a long period.

Because of the need to take account of complex coorbital flows in a partially gap forming regime close to the planet, the problem of type III migration is very numerically challenging and therefore not unexpectedly issues of adequate numerical resolution and convergence remain outstanding.

D'Angelo et al. (2005) have undertaken numerical simulations of runaway migration using a nested grid system that can give high resolution within the Roche lobe, but not elsewhere in the simulation, and found that the outcome, stated to be the suppression of type III migration, was highly dependent on the torque calculation prescription (more precisely on whether the Roche lobe material was taken into account or not in this calculation) and on the mesh resolution. One of the main subtleties of coorbital dynamics is to properly take into account the inertia of all the material trapped (even approximately) in libration with the planet, be it the horseshoe or circumplanetary material. Including the Roche lobe material in the torque calculation, while for other purposes it is assumed to be non self-gravitating, introduces a discrepancy between the inertial mass of the migrating object (the point like object plus the Roche lobe content) and its active gravitational mass (the mass of the point like object). This unphysical discrepancy can be large and severely alter the migration properties, especially at high resolution where the Roche lobe is flooded by disk material in a manner than strongly depends on the equation of state. On the other hand *Masset and Papaloizou (2003)* consider the Roche lobe content as a whole, referred to as the planet for simplicity, assuming that for a given mass M_p' of this object, there always exists a point-like object with mass $M_p < M_p'$ such that the whole Roche lobe content has mass M_p' . In this case, one needs to exclude the Roche lobe content from the torque calculation (since the forces originating from within the Roche lobe are not external forces), and this way one naturally gets inertial and active gravitational masses of the Roche lobe content (migrating object) that both amount to M_p' .

Another way of looking at this issue is to realize that from considerations of angular momentum conservation, the angular momentum changes producing the migration can be evaluated at large distances from the Roche lobe. Suppose that the material inside the Roche lobe had some asymmetric structure that produced a torque on the point like mass M_p . Then in order to sustain this structure in any kind of steady state, external interaction would have to provide an exactly counterbalancing torque that could be measured in material exterior to the Roche lobe (for more details see the review by *Papaloizou and Terquem, 2006*).

In addition to the above issues, the effect of viscosity on the libration region through its action on the specific vorticity profile or the consequences of specific vorticity generation at gap edges (e.g., *Koller et al., 2005*) has yet to be considered.

Potential consequences for forming planets. The Minimum Mass Solar Nebula (MMSN) is not massive enough to allow giant planets to experience runaway migration. This is most likely for planets with masses comparable to that of Saturn in disks that do not need to be more massive than a few times the Minimum Mass Solar Nebula.

Thus runaway migration should it occur makes the tendency for the migration rate to be a maximum, in the mass range associated with the onset of gap formation and type II

migration, more pronounced. This may be related to the fact that most of the extrasolar planets known as “hot Jupiters”, with a semi-major axis $a < .06$ AU, happen to have sub-Jovian masses. Assuming that type I migration is suppressed by, e.g., MHD turbulence (see below) a forming protoplanet, as it passes through the domain of fast migration, would migrate very fast towards the central object and at the same time it would accrete gas from the nebula. If the protoplanet is able to form a deep gap before it reaches the central regions of the disk, or stellar magnetosphere, it enters the slow, type II migration regime, having at least about a Jupiter mass. Otherwise, it reaches the central regions still as a sub-Jovian object.

5. TURBULENT PROTOPLANETARY DISKS

The majority of calculations examining the interaction between protoplanets and protoplanetary discs have assumed that the disc is laminar. The mass accretion rates inferred from observations of young stars, however, require an anomalous source of viscosity to operate in these discs. The most likely source of angular momentum transport is magnetohydrodynamic turbulence generated by the magnetorotational instability (MRI) (*Balbus and Hawley, 1991*). Numerical simulations performed using both the local shearing box approximation (see *Balbus and Hawley, 1998* for a review) and global cylindrical disc models (e.g., *Papaloizou and Nelson, 2003* and references therein) indicate that the nonlinear outcome of the MRI is vigorous turbulence, and dynamo action, whose associated stresses can account for the observed accretion rates inferred for T Tauri stars.

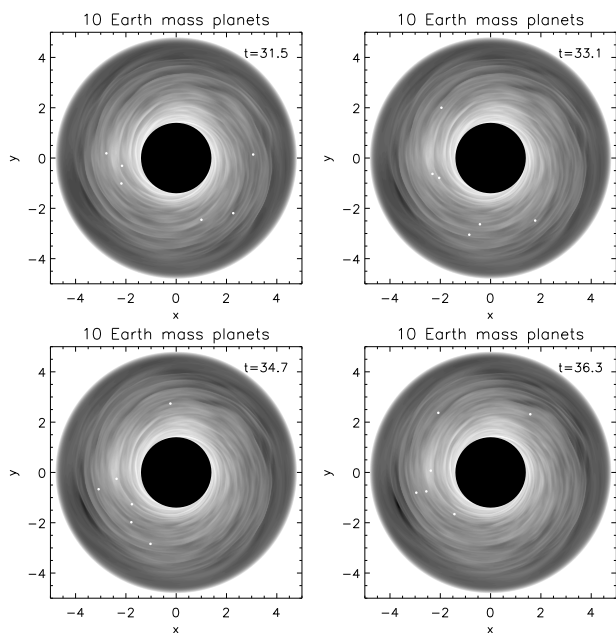


Fig. 9.— This figure shows the orbital evolution of six $10 M_{\oplus}$ protoplanets embedded in a turbulent protoplanetary disc.

These studies assumed that the approximation of ideal MHD was appropriate. The ionisation fraction in cool, dense protoplanetary discs, however, is probably small in the planet forming region between 1 – 10 AU. Only the surface layers of the disc, which are exposed to external sources of ionisation such as X-rays from the central star or cosmic rays, are likely to be sufficiently ionised to sustain MHD turbulence (e.g., *Gammie, 1996; Fromang et al., 2002*). However, this involves complex chemical reaction networks and the degree of depletion of dust grains which itself may vary while there is ongoing planet formation.

Recent work has examined the interaction between planets of various masses and turbulent protoplanetary discs. These studies have usually simulated explicitly MHD turbulence arising from the MRI. We now review the results of these studies.

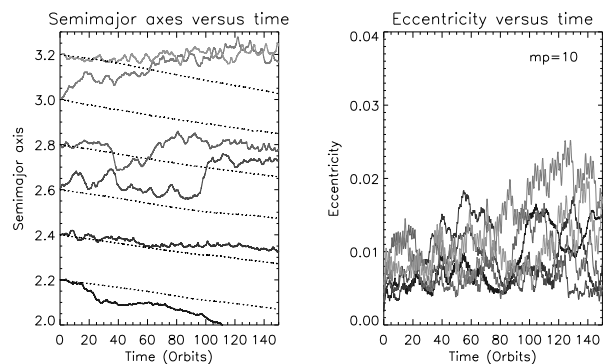


Fig. 10.— The left panel shows the variation of semimajor axis with time (measured in planet orbits at $r = 2.3$). The dotted lines represent the trajectories of $10 M_{\oplus}$ planets in equivalent laminar discs. The right panel shows the variation of eccentricity. For $10 M_{\oplus}$ bodies, eccentricity damping due to coorbital Lindblad torques maintains low eccentricities.

5.1. Low mass protoplanets in turbulent discs

The interaction between low mass, non gap forming protoplanets and turbulent discs has been examined by *Papaloizou et al. (2004)*, *Nelson and Papaloizou (2004)*, *Nelson (2005)* and *Laughlin et al. (2004)*. These calculations show that interaction between embedded planets and density fluctuations generated by MHD turbulence can significantly modify type I migration, at least over time scales equal to the duration of simulations that are currently feasible ($t \sim 150$ planet orbits). leading to a process of ‘stochastic migration’ rather than the monotonic inward drift expected for planets in laminar discs. Figure 9 shows snapshots of the midplane density for six $10 M_{\oplus}$ planets (non interacting) embedded in a turbulent disc with $H/R = 0.07$, and show that the turbulent density fluctuations are of higher amplitude than the spiral wakes generated by the planet (*Nelson and Papaloizou, 2004; Nelson, 2005*). Indeed, typical surface density fluctuations generated by tur-

bulence in simulations are typically $\delta\Sigma/\Sigma \simeq 0.15 - 0.3$, with peak fluctuations being $\mathcal{O}(1)$. Thus, on the scale of the disc thickness H , density fluctuations can contain more than an Earth mass in a disc model a few times more massive than a minimum mass nebula.

Figure 10 shows the variation in the semimajor axes of the planets shown in figure 9, and figure 11 shows the running mean of the torque for one of the planets. It is clear that the usual inward type I migration is disrupted by the turbulence, and the mean torque does not converge toward the value obtained in a laminar disc for the duration of the simulation. A key question is whether the stochastic torques can continue to overcome type I migration over time scales up to disc life times. A definitive answer will require very long global simulations.

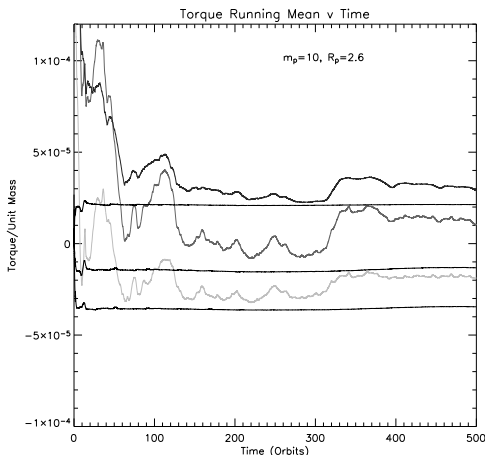


Fig. 11.— This figure shows the running time average of the torque per unit mass for the planet in figs. 9 and 10 whose initial orbit is at $r = 2.6$. The ultimately lowest but not straight line corresponds to the torque exerted by the outer disc, the ultimately uppermost line corresponds to the inner disc torque, and the line ultimately between them corresponds to the total torque. The three horizontal lines correspond to the inner, outer and total torque exerted on a planet in laminar disc.

One can test the possibility that the response of the turbulent disc is that of a laminar disc whose underlying density is given by the time averaged value, superposed on which are Gaussian distributed fluctuations with a characteristic recurrence time \sim the orbital period. If such a picture applies then the time averaged torque experienced by the protoplanet, \bar{T} , can be expressed as

$$\bar{T} = \langle T \rangle + \frac{\sigma_T}{\sqrt{t_{tot}}} \quad (22)$$

where σ_T is the standard deviation of the torque amplitude, $\langle T \rangle$ is the underlying type I torque, and t_{tot} is the total time elapsed, measured in units of the characteristic time for the torque amplitude to vary. Convergence toward the

underlying type I value is expected to begin once the two terms on the right hand side become equal. For $10 M_{\oplus}$ protoplanets, simulations indicate that $\sigma_T \simeq 10 < T \rangle$, with a simple estimate of the time for fluctuations to recur being $\simeq 1/2$ the planet orbital period (Nelson and Papaloizou, 2004; Nelson, 2005). The torque convergence time is then $\simeq 50$ planet orbits. Interestingly, the simulations presented in figure 10 were run for $\simeq 150$ planet orbits, and do not show a tendency for inward migration.

Analysis of the stochastic torques suggests that they vary on a range of characteristic times from the orbital period to the run times of the simulations themselves (Nelson, 2005). This feature can in principle allow a planet to overcome type I migration for extended time periods. It appears to at least partially explain why the simulations do not show inward migration on the time scale predicted by Eq. 22. The origin of these long time scale fluctuations is currently unknown.

Additionally, the picture described above of linear superposition of stochastic fluctuations on an underlying type I torque may not be correct due to non linear effects. Density fluctuations occurring within the disc in the planet vicinity are substantial, such that the usual bias between inner and outer type I torques may not be recovered easily, invalidating the assumptions leading to Eq. 22. To see this, consider a density fluctuation of order unity with length scale of order H a distance of order H from the planet. The characteristic specific torque acting on it is $G\Sigma R$. Given their stochastic nature, one might expect the specific torque acting on the planet to oscillate between $\pm G\Sigma R$. Note that this exceeds the net specific torque implied by Eq. (9) by a factor $T_f \sim [(M_*/M_p)(h)^3]h^{-1}$. From the discussion in section 3, the first factor should exceed unity for an embedded planet. Thus, such an object is inevitably subject to large torque fluctuations. The strength of the perturbation of the planet on the disk is measured by the dimensionless quantity $(M_p/M_*)(h)^{-3}$. This perturbation might be expected to produce a bias in the underlying stochastic torques. If it produces a non zero mean, corresponding to the typical fluctuation reduced by a factor T_f , this becomes comparable to the laminar type I value. However, there is no reason to suppose the exact type I result should be recovered. But note the additional complication that the concept of such a mean may not have much significance in practical cases, if large fluctuations can occur on the disk evolutionary timescale, such that it is effectively not established.

We comment that, as indicated in the plots in figure 11 at small times, the one sided torque fluctuations can be more than an order of magnitude larger than expected type I values. However, such fluctuations occur on an orbital timescale and if averages over periods of 50 orbits are considered values more like type I values are obtained. Accordingly, the large fluctuations are not associated with large orbital changes.

Further work is currently underway to clarify the role of turbulence on modifying type I migration, including type I migration in vertically stratified turbulent discs.

5.2. High mass protoplanets in turbulent discs

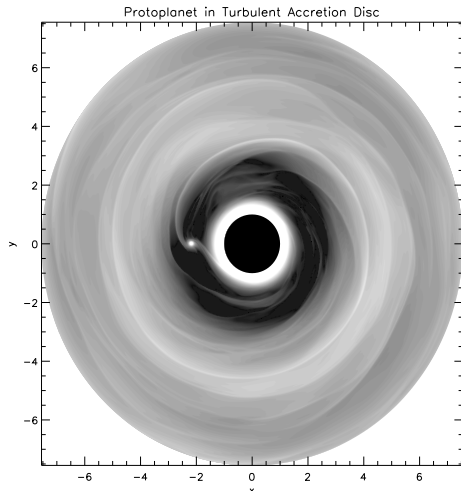


Fig. 12.— This figure shows a snapshot of the disc midplane density for a $5 M_{\text{Jupiter}}$ protoplanet embedded in a turbulent disc.

The interaction of high mass, gap forming planets with turbulent protoplanetary discs has been considered in a number of papers (*Nelson and Papaloizou, 2003; Winters et al., 2003; Papaloizou et al., 2004; Nelson and Papaloizou, 2004*). Figure 12 shows the midplane density for a turbulent disc with an embedded $5 M_{\text{Jupiter}}$ protoplanet. As expected from the discussion presented in section 3, gap formation occurs because the Roche lobe radius exceeds the disc scale height, and tidal torques locally overwhelm viscous torques in the disc.

Papaloizou et al. (2004) considered the transition from fully embedded to gap forming planets using local shearing box and global simulations of turbulent discs. These simulations showed that gap formation begins when $(M_p/M_*)(R/H)^3 \simeq 1$, which is the condition for the disc response to the planet gravity being non linear. The viscous stress in simulations with zero-net magnetic flux (as normally considered here) typically give rises to an effective $\alpha \simeq 5 \times 10^{-3}$, such that the viscous criterion for gap formation is satisfied when the criterion for non linear disc response is satisfied.

Global simulations allow the net torque on the planet due to the disc to be calculated and hence the migration time to be estimated. Simulations presented in *Nelson and Papaloizou (2003, 2004)* for massive planets indicate migration times of $\sim 10^5$ yr, in line with expectations for type II migration.

A number of interesting features arise in simulations of gap forming planets embedded in turbulent discs. The magnetic field topology is significantly modified in the vicinity of the protoplanet, as illustrated by figure 13. The field is compressed and ordered in the postshock region associated with the spiral wakes, increasing the magnetic stresses there. Accretion of gas into the protoplanet Hill sphere

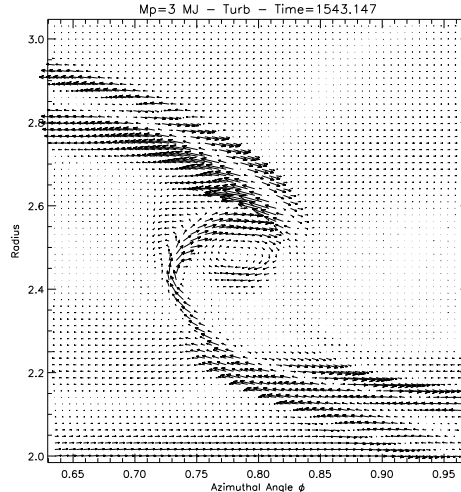


Fig. 13.— This figure shows magnetic field lines in the vicinity of the protoplanet. Field lines link the protoplanetary disc with the circumplanetary disc within the planet Hill sphere.

causes advection of field into the circumplanetary disc that forms there, and this field then links between the protoplanetary disc and the circumplanetary disc, apparently contributing to magnetic braking of the circumplanetary material. Indeed, comparison between a simulation of a $3 M_{\text{Jupiter}}$ protoplanet in a viscous laminar disc and an equivalent turbulent disc simulation suggests that mass accretion onto the planet may be enhanced by this effect. Figure 14 shows the average density in the vicinity of the planet for a laminar disc run and a turbulent disc simulation, indicating that the softened point mass used to model the planet has accreted more gas in the turbulent disc run. In addition, the gap generated tends to be deeper and wider in turbulent discs than in equivalent viscous, laminar discs (*Nelson and Papaloizou, 2003; Papaloizou et al., 2004*). It is worth noting, however, that the global simulations are of modest resolution, and more high resolution work needs to be done to examine these issues in greater detail.

6. SUMMARY AND DISCUSSION

We have reviewed recent progress in the field of disk planet interactions in the context of orbital migration. This has mainly come from large scale two and three dimensional simulations that have utilised the most up to date supercomputer resources. These have allowed the application of high resolution multigrid methods and the study of disks with MHD turbulence interacting with planets. Simulations of both laminar and turbulent discs have been carried out and while the structure of the protoplanetary disk is uncertain, both these types are valuable.

In the case of type I migration it has become clear that the 3D simulations discussed above agree with results obtained from linear analysis and summing contributions from resonant torques (*Tanaka et al., 2002*) in predicting that

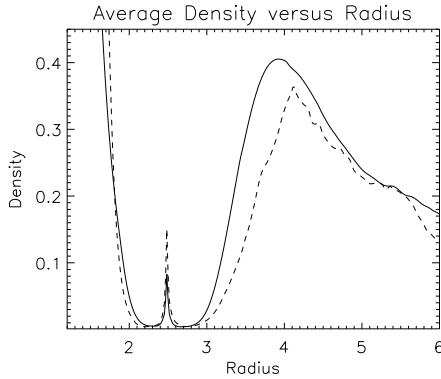


Fig. 14.— The average density in the vicinity of the planet as a function of radius for a laminar viscous disk (solid line) and for a disk with MHD turbulence (dashed line). More mass has settled onto the planet in the latter case possibly due to magnetic braking.

planets in the M_{\oplus} range in axisymmetric smoothly varying laminar disks, modelling the minimum mass solar nebula, undergo a robust inward migration on a $10^6 y$ timescale. This is a threat to the viability of the core accumulation scenario and a resolution has to be sought.

Several potential resolutions involving departures from the simple disk model have been suggested. These include invoking sharp radial opacity variations (*Menou and Goodman, 2004*), large scale nonaxisymmetric distortions (e.g., an eccentric disc) (*Papaloizou, 2002*) or a large scale toroidal magnetic field *Terquem, (2003)*.

If the disk is magnetically active, type I drift may be disrupted by stochastic migration even for very extended periods of time (*Nelson and Papaloizou, 2004*). Even if this is unable to keep type I migration at bay for the entire disk lifetime, the increased mobility of the cores may have important consequences for their build up through accretion (*Rice and Armitage, 2003*).

But note that even within the context of laminar disks, simulations have revealed that type I migration has to be suppressed in the $10M_{\oplus}$ range by weak nonlinear effects (*D'Angelo et al., 2003a*).

Gap formation in a standard MMSN disk is found to occur for planets with mass exceeding that of \sim Saturn, at which mass the migration rate is a maximum leading to an infall time of $3 \times 10^4 y$. Beyond that mass the rate decreases with the onset of type II migration on the viscous time scale. In more massive disks the maximum migration rate at a Saturn mass is potentially enhanced by the positive feedback from coorbital torques leading to a fast type III migration regime (*Masset and Papaloizou, 2003; Artymowicz, 2004*). However the operation of coorbital torques requires to be clarified with further high resolution studies. But it is nonetheless interesting to speculate that the maximum migration rate at a Saturn mass is connected to the 'hot Jupiters' which tend to have sub Jovian masses (see section 4 above). Once gap formation has occurred, type II mi-

gration ensues which appears to allow models that assume formation beyond the snow line to produce giant planet distributions in accord with observations (e.g., *Trilling et al., 1998; 2002; Alibert et al., 2004*).

REFERENCES

- Alibert Y., Mordasini C., and Benz W. (2004) *Astron. Astrophys.*, 417, L 25-L 28.
- Armitage P. J., Livio M., Lubow S. H., and Pringle J. E. (2002) *Mon. Not. R. Astr. Soc.*, 334, 248-256.
- Artymowicz P. (1993) *Astrophys. J.*, 419, 155-165.
- Artymowicz P. (2004) *Publ. Astr. Soc. Pac.*, 324, 39-49.
- Artymowicz P. (2006) *In preparation*
- Balbus S. A. and Hawley J. F. (1991) *Astrophys. J.*, 376, 214-233.
- Balbus S. A. and Hawley J. F. (1998) *Rev. Mod. Phys.*, 70, 1-53.
- Balmforth N. J. and Korycansky D. G. (2001) *Mon. Not. R. Astr. Soc.*, 316, 833-851.
- Bate M. R., Lubow S. H., Ogilvie G. I., and Miller K. A. (2003) *Mon. Not. R. Astron. Soc.*, 341, 213-229.
- Bryden G., Chen X., Lin D. N. C., Nelson R. P., and Papaloizou J. C. B. (1999) *Astrophys. J.*, 514, 344-367.
- Crida A., Morbidelli A., and Masset F. S., (2006) *Icarus, in press*, astro-ph/0511082.
- D'Angelo G., Bate M., and Lubow S. (2005) *Mon. Not. R. Astr. Soc.*, 358, 316-332.
- D'Angelo G., Henning T., and Kley W. (2002) *Astron. Astrophys.*, 385, 647-670.
- D'Angelo G., Henning T., and Kley W. (2003a) *Astrophys. J.*, 599, 548-576.
- D'Angelo G., Kley W., and Henning T. (2003b) *Astrophys. J.*, 586, 540-561.
- Fromang S., Terquem C., and Balbus S. A. (2002) *Mon. Not. R. Astron. Soc.*, 329, 18-28.
- Gammie C. F. (1996) *Astrophys. J.*, 457, 355-362.
- Goldreich P. and Sari R. (2003) *Astrophys. J.*, 585, 1024-1037.
- Goldreich P. and Tremaine S. (1979) *Astrophys. J.*, 233, 857-871.
- Ida S. and Lin D. N. C. (2004) *Astrophys. J.*, 616, 567-572.
- Ivanov P. B., Papaloizou J. C. B., and Polnarev A. G. (1999) *Mon. Not. R. Astron. Soc.*, 307, 79-90.
- Jang-Condell H., Sasselov D. D. (2005) *Astrophys. J.*, 619, 1123-1131.
- Kley W. (1999) *Mon. Not. R. Astron. Soc.*, 303, 696-710.
- Koller J., Li H. and Lin D. N. C. (2003) *Astrophys. J.*, 596, L 91-L 94.
- Korycansky D. G. and Pollack J. B. (1993) *Icarus*, 102, 150-165.
- Laughlin, G., Steinacker A., and Adams F. C. (2004) *Astrophys. J.*, 608, 489-496.
- Lin D. N. C. and Papaloizou J. C. B. (1979) *Mon. Not. R. Astron. Soc.*, 186, 799-830.
- Lin D. N. C. and Papaloizou J. C. B. (1986) *Astrophys. J.*, 309, 846-857.
- Lin D. N. C. and Papaloizou J. C. B. (1993) In *Protostars and Planets III* (E. H. Levy and J. I. Lunine eds.), pp. 749-835, Univ. of Arizona, Tucson.

- Lin D. N. C., Papaloizou J. C. B., Terquem C., Bryden G., and Ida S. (2000) In *Protostars and Planets IV* (V. Mannings et al. eds.), pp. 1111-1134, Univ. of Arizona, Tucson.
- Lubow S. H., Seibert M., and Artymowicz P. (1999) *Astrophys. J.*, 526, 1001-1012.
- Marcy G. W. and Butler R. P. (1995) *187th AAS Meeting BAAS.*, 27, 1379-1384.
- Marcy G. W. and Butler R. P. (1998) *Ann. Rev. Astron. Astr.*, 36, 57-97.
- Mayor, M. and Queloz, D. (1995) *Nature*, 378, 355-359.
- Masset F. (2001) *Astrophys. J.*, 558, 453-462.
- Masset F. (2002) *Astron. Astrophys.*, 387, 605-623.
- Masset F. S., D'Angelo G., and Kley W. (2006) *In preparation*.
- Masset F. and Papaloizou J. C. B. (2003) *Astrophys. J.*, 588, 494-508.
- Mayor M. and Queloz D. (1995) *Nature*, 378, 355-359.
- Menou K. and Goodman J. (2004) *Astrophys. J.*, 606, 520-531.
- Nelson A. F. and Benz W. (2003) *Astrophys. J.*, 589, 578-604.
- Nelson R. P. (2005) *Astron. Astrophys.*, 443, 1067-1085.
- Nelson R. P. and Papaloizou J. C. B. (2003) *Mon. Not. R. Astron. Soc.*, 339, 993-1005.
- Nelson R. P. and Papaloizou J. C. B. (2004) *Mon. Not. R. Astron. Soc.*, 350, 849-864.
- Nelson R. P., Papaloizou J. C. B., Masset F., and Kley W. (2000) *Mon. Not. R. Astron. Soc.*, 318, 18-36.
- Ogilvie G. I. and Lubow S. H. (2003) *Astrophys. J.*, 587, 398-406.
- Papaloizou J. C. B. (2002) *Astron. Astrophys.*, 388, 615-631.
- Papaloizou J. C. B. (2005) *Celest. Mech. Dyn. Astron.*, 91, 33-57.
- Papaloizou J. C. B. and Larwood J. D. (2000) *Mon. Not. R. Astron. Soc.*, 315, 823-833.
- Papaloizou J. C. B. and Nelson R. P. (2003) *Mon. Not. R. Astron. Soc.*, 350, 983-992.
- Papaloizou J. C. B. and Nelson R. P. (2005) *Astron. Astrophys.*, 433, 247-265.
- Papaloizou J. C. B., Nelson R. P., and Snellgrove M. D. (2004) *Mon. Not. R. Astron. Soc.*, 350, 829-848.
- Papaloizou J. C. B. and Terquem C. (2006) *Rep. Prog. Phys.*, 69, 119-180.
- Pierens A. and Huré J. M. (2005) *Astron. Astrophys.*, 433, L 37-L 40.
- Rice W. K. M. and Armitage P. J. (2003) *Astrophys. J.*, 598, L 55-L 58.
- Syer D. and Clarke C. J. (1995) *Mon. Not. R. Astron. Soc.*, 277, 758-766.
- Tanaka H., Takeuchi T., and Ward W. R. (2002) *Astrophys. J.*, 565, 1257-1274.
- Terquem C. E. J. M. L. J. (2003) *Mon. Not. R. Astron. Soc.*, 341, 1157-1173.
- Trilling D. E., Benz W., Guillot T., Lunine J. I., Hubbard W. B., and Burrows A. (1998) *Astrophys. J.*, 500, 428-439.
- Trilling D. E., Lunine J. I., and Benz W. (2002) *Astron. Astrophys.*, 394, 241-251.
- Ward W. R. (1997) *Icarus*, 126, 261-281.
- Winters, W. F., Balbus S. A., and Hawley, J. F. (2003) *Astrophys. J.*, 589, 543-555.